JOURNAL OF MATERIALS SCIENCE 29 (1994) 2491–2499

# Microstructural evolution and calorimetric evaluation of non-equilibrium states in rapidly solidified Al–Mn–Co ternary alloys

YIBIN ZHANG, TOSHIMI YAMANE, SHIGEOKI SAJI
*Department of Materials Science and Engineering, Faculty of Engineering, Osaka University, 2-1, Yamadaoka, Suita, Osaka 565, Japan*

JUNZO TAKAHASHI
*Department of Dental Technology, Faculty of Dentistry, Osaka University, 1-8, Yamadaoka, Suita, Osaka 565, Japan*

Evolutionary structures were observed in as-melt spun ribbons of Al–3.5Mn–0.8Co, Al–3.5Mn–1.3Co, Al–3.5Mn–2Co, Al–5Mn–0.8Co and Al–5Mn–2Co alloys. The evolutionary structures contained two zones, zone A and zone B, at the chilled and unchilled sides, respectively. A banded structure was observed between the two zones as a transitional region in the Al–3.5Mn–1.3Co alloy. The enthalpy differences, $\Delta H_0^{ne}$, between a non-equilibrium state in as-melt spun ribbons and the equilibrium state in fully annealed ribbons of the Al–Mn–Co alloys were evaluated using data obtained by differential scanning calorimetry (DSC) measurements. The values of $\Delta H_0^{ne}$ for Al–Mn–Co alloys are lower than those for Al–Mn binary alloys. $\Delta H_0^{ne}$ corresponds to a decrease in Gibbs free energy, $\Delta G$, which is stored in a solidified solid during rapid solidification. The formation of the banded structure is interpreted on the basis of an analysis of the distribution of $\Delta H_0^{ne}$ or the fluctuation in $\Delta G$, which should oscillate in order to correspond with a gradual reduction of cooling ability for the constrained solidification by the substrate.

## 1. Introduction

The structural evolution of rapidly solidified powders, ribbons and electron-beam samples of Al–Fe and Al–Fe base alloys has been described in several reports [1–5]. In particular, the ribbons showed a structural evolution from zone A, a fine structural region at the chilled side, to the zone B, an etch-sensitive region which appeared extensively on the unchilled side [1]. Evolution of this kind of two-zone structure has also even been recognized in Al–Cu alloys near the Al–$Al_2Cu$ equilibrium eutectic composition [6]. A banded structure, a region of the structural evolution, consisting of a regular succession of dark and light bands, has been observed in Ag–Cu, Al–Cu and Al–Fe alloys [7–12]. Rapidly solidified Al–Mn and Al–Mn–X (where X is a transition metal) alloys exhibited a complex structure, and formed two quasicrystalline phases, that is, icosahedral and decagonal phases [13–18]. No work on rapidly solidified Al–Mn–Co alloys has been reported.

Rapid solidification produces a non-equilibrium state in an alloy system; then, an enthalpy difference, $\Delta H_0^{ne}$, exists between as-rapidly-solidified ribbons and fully annealed ribbons at room temperature. In a previous work [16], we proposed a method to evaluate this enthalpy difference using a technique based on the differential scanning calorimetry (DSC) measurements, and we established the values of $\Delta H_0^{ne}$ in as-melt spun Al–1.66, 2.56, 3.95, 5.45 and 6.98 at % Mn alloys.

The present work aimed to investigate the microstructural evolution and features in as-melt spun Al–Mn–Co alloys, to evaluate the values of $\Delta H_0^{ne}$ and to explain the microstructural evolution on the basis of an analysis of thermodynamic aspects of $\Delta H_0^{ne}$.

## 2. Experimental procedures

The five Al–Mn–Co alloys used in this study were prepared by melting 99.993 wt % pure Al, 99.99 wt % pure Mn and 99.9 wt % pure Co in alumina crucibles; the compositions of these alloys are shown in Table I. Using a melt-spinning device, those alloys molten at temperatures higher than 1100 K were squirted with argon gas of 80 kPa pressure on a copper roller, which was 153 mm in diameter and rotated at a surface velocity of 38 $m\,s^{-1}$. The continuous ribbons obtained had a sectional shape 3–4 mm wide and 45–55 μm thick. This single roller method was considered to produce a cooling rate of $10^5$–$10^6$ $K\,s^{-1}$ for ribbons 30 μm thick [9].

Microstructural observations were performed by transmission electron microscopy (TEM) operated at 125 kV for specimens thinned by a twin-jet electropolishing method in a methanol solution containing 8 wt % $HClO_4$ and 37 vol % glycerin and by

0022–2461 

TABLE I Chemical compositions of the Al–Mn–Co alloys

| Alloys | Compositions (at %) | | |
|---|---|---|---|
| | Mn | Co | Al |
| Al–3.5Mn–0.8Co | 3.48 | 0.78 | Balance |
| Al–3.5Mn–1.3Co | 3.38 | 1.30 | Balance |
| Al–3.5Mn–2Co | 3.44 | 2.07 | Balance |
| Al–5Mn–0.8Co | 4.99 | 0.84 | Balance |
| Al–5Mn–2Co | 4.97 | 2.04 | Balance |

scanning electron microscopy (SEM) operated at 15 kV for transverse sections of ribbons.

The values of $\Delta H_0^{ne}$ were evaluated approximately on the basis of DSC measurements, which were carried out in two runs at a heating rate of 0.2 K $s^{-1}$ from 310 to 870 K, $T_a$ and $T_b$, respectively. The instrument's constant for the DSC apparatus was determined by measuring the heat of fusion and the melting point of pure Sn, Zn and Pb. As-melt spun ribbon of 37 to 38 mg and 99.993 wt % pure Al of 40 mg (as a reference sample) in weight were individually packed in Al pans for the DSC measurements. $\Delta H_0^{ne}$ can be expressed in the following differential form

$$\frac{d(\Delta H_0^{ne})}{dT} = \left(\frac{\kappa}{\beta}\right)[D^{ne}(T) - D^{e}(T)] \quad (1)$$

where, $\beta$ is the heating rate of the DSC measurement, $\kappa$ is the instrument's constant, $D^{ne}(T)$ is the first-DSC-run signal of an as-melt spun ribbon, $D^{e}(T)$ is the second-DSC-run signal, and the samples were fully annealed between the first and second DSC runs. The value of $\Delta H_0^{ne}$ was calculated by a definite integral of Equation 1

$$\Delta H_0^{ne} = \int_{T_a}^{T_b} \left(\frac{\kappa}{\beta}\right)[D^{ne}(T) - D^{e}(T)]\,dT \quad (2)$$

We will refer to the curve represented by Equation 1 as a $d(\Delta H_0^{ne})/dT$–$T$ curve [16]. Another enthalpy change, $\Delta H_0^{ne'}$ is usually ascribed to phase transformation during heating, and it can be estimated from area integration of peaks on the $d(\Delta H_0^{ne})/dT$–$T$ curve.

## 3. Experimental results

### 3.1. SEM microstructures in the transverse section of ribbons

Fig. 1 shows SEM micrographs observed in the transverse section of as-melt spun ribbons. The microstructure exhibited two zones: *zone A*, a fine structural region at the chilled side in the five alloys; and *zone B*, an etch-sensitive region with coarse particles and dendritic cells at the unchilled side, as shown in Fig. 1 (a), (b), (c) and (d) for four alloys. Many grains having one core can be seen; this is indicated by arrows in Fig. 1e for the Al–5Mn–2Co alloy. For the

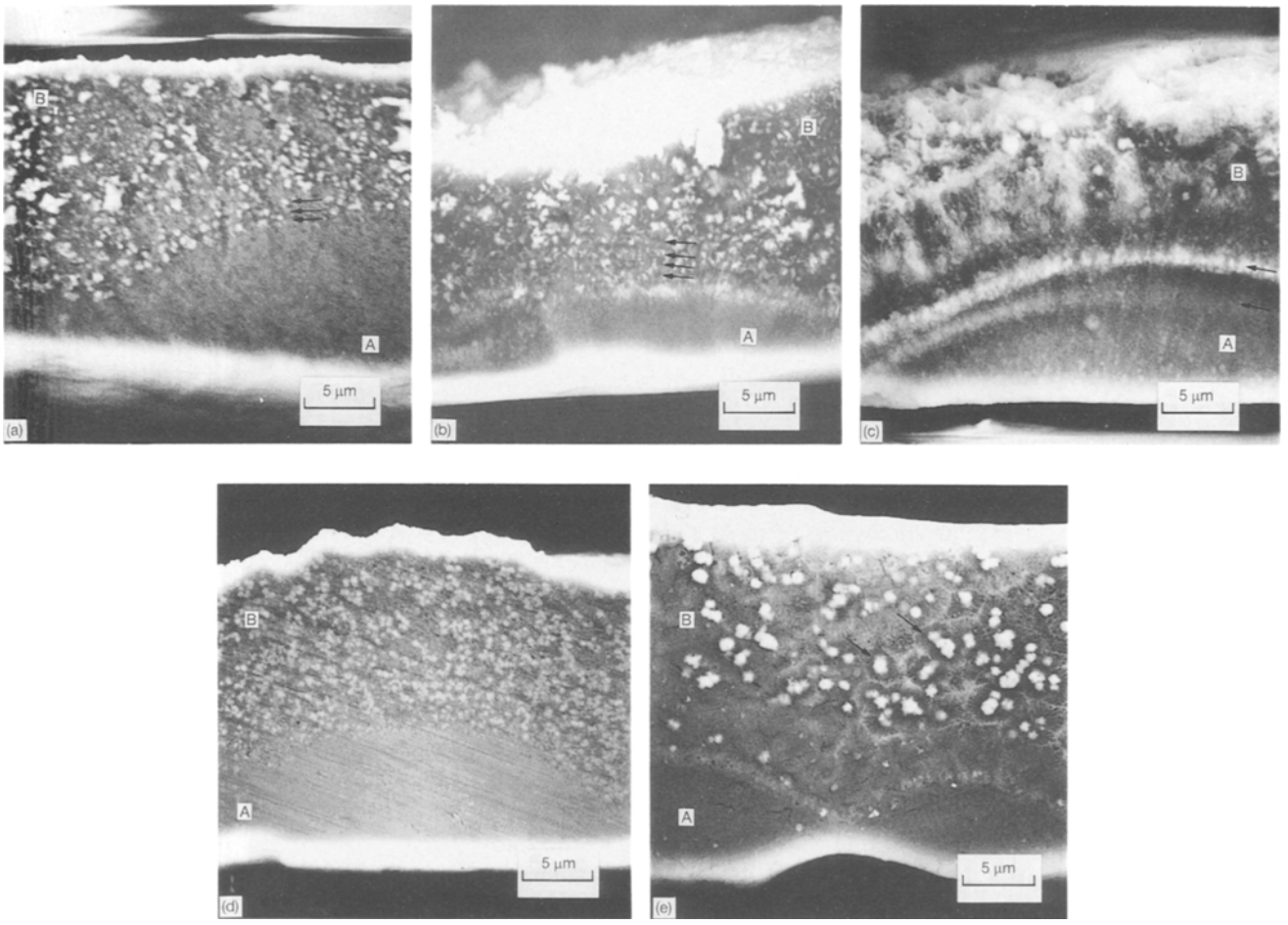


*Figure 1* SEM micrographs of as-melt spun ribbons in transverse section. A denotes zone A and B denotes zone B. (a) Al–3.5Mn–0.8Co alloy, (b) Al–3.5Mn–1.3Co alloy, (c) Al–3.5Mn–2Co alloy, (d) Al–5Mn–0.8Co alloy, and (e) Al–5Mn–2Co alloy. The chilled sides are at the bottom of the micrographs.

Al–3.5Mn–0.8Co, Al–3.5Mn–1.3Co and Al–3.5Mn–2Co alloys, an alternate arrangement of different structural layers, marked by arrows in Fig. 1a–c, can be seen as a transition region between zones A and B. This may suggest the existence of a banded structure. In observations with an optical microscope, this transitional region exhibited mottled "growth rings", which depended on the Co content.

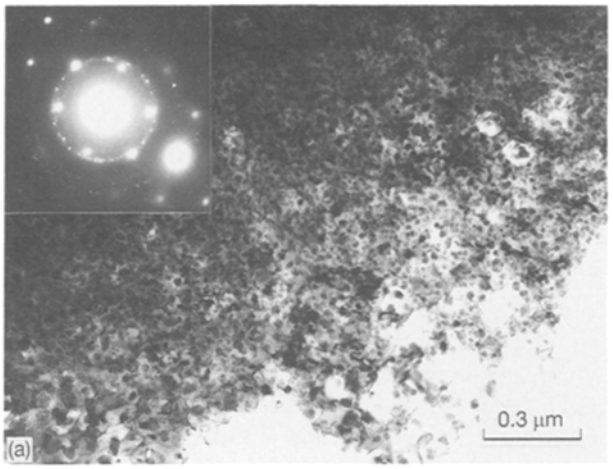


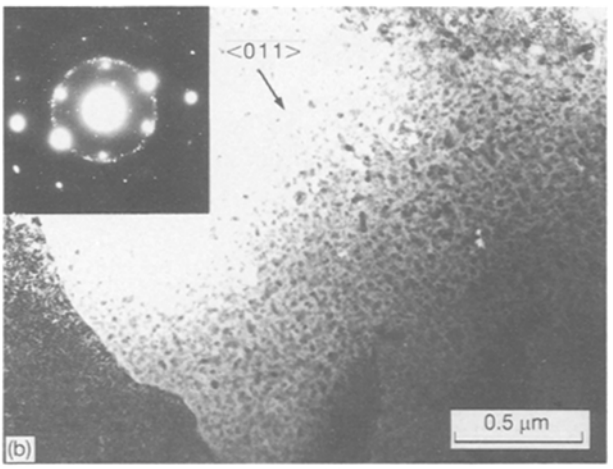


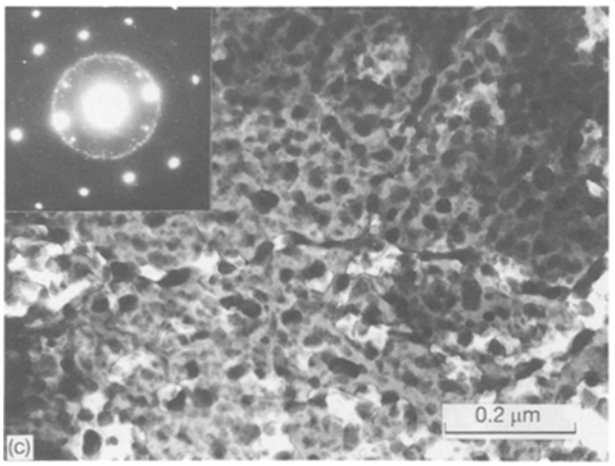


*Figure 2* TEM microstructures of zone A. SAD revealed a spotty ring pattern of $Al_9Co_2$ overlapping a SAD pattern of the α-Al matrix: (a) Al–3.5Mn–0.8Co alloy with a SAD pattern of the $[0\bar{2}2]_{\alpha\text{-Al}}$-zone axis, (b) Al–3.5Mn–1.3Co alloy with a SAD pattern of the $[0\bar{2}2]_{\alpha\text{-Al}}$-zone axis, (c) Al–3.5Mn–2Co alloy with a SAD pattern of the $[\bar{1}12]_{\alpha\text{-Al}}$-zone axis.

## 3.2. TEM microstructures

### *3.2.1. Zone A*

Typical TEM microstructures and selected-area-diffraction (SAD) patterns of zone A in Al–3.5Mn–0.8Co, Al–3.5Mn–1.3Co and Al–3.5Mn–2Co alloys are shown in Fig. 2a–c, respectively. It is found that extremely refined, homogeneous particles (less than 30 nm in diameter) are dispersed within the grains. The SAD patterns from zone A show that the matrix is α-Al grains over a large area and that the dispersoids are randomly oriented particles of $Al_9Co_2$. The amount of the $Al_9Co_2$ particles increased with increasing Co content.

Fig. 3a and b shows TEM microstructures and SAD patterns of zone A in Al–5Mn–0.8Co and Al–5Mn–2Co alloys. Many dispersoids are also observed within the α-Al grains; the spotty rings, indicated by arrows in the SAD pattern, correspond to diffraction spots of the icosahedral phase, and some diffraction spots show the existence of $Al_9Co_2$ particles.

The microstructures of the zone A were characterized by extremely refined, homogeneous, randomly oriented particles in the α-Al grains. This structure is

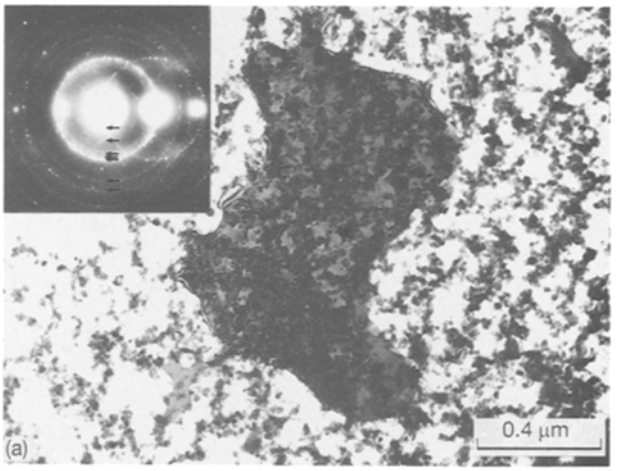


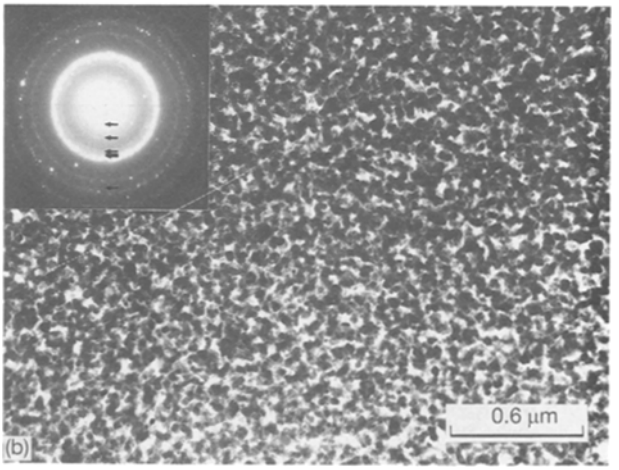


*Figure 3* TEM microstructures of zone A showing dispersoids of the icosahedral phase and $Al_9Co_2$ within the α-Al grains. (a) An Al–5Mn–0.8Co alloy, the SAD pattern from the centre shows dense spotty rings of the icosahedral phase and of $Al_9Co_2$; they overlap a pattern from the $[1\,3\,4]_{\alpha\text{-Al}}$-zone axis. (b) Particles after elution of the α-Al matrix in an Al–5Mn–2Co alloy; the SAD pattern exhibits spotty rings of the icosahedral phase and $Al_9Co_2$.

similar to the structure which was observed in rapidly solidified Al–Fe, Al–Fe–Ni and Al–Fe–Si alloys [1–5].

### 3.2.2. Zone B

TEM microstructures of zone B in Al–3.5Mn–0.8Co, Al–3.5Mn–1.3Co and Al–3.5Mn–2Co alloys are shown in Fig. 4. The rhombic branches marked A in Fig. 4a were confirmed as $Al_9Co_2$ in the Al–3.5Mn–0.8Co alloy; they are also observed in the Al–3.5Mn–1.3Co and Al–3.5Mn–2Co alloys. The particles marked B in Fig. 4a were $Al_6Mn$, and the particle clusters marked C were the icosahedral phase.

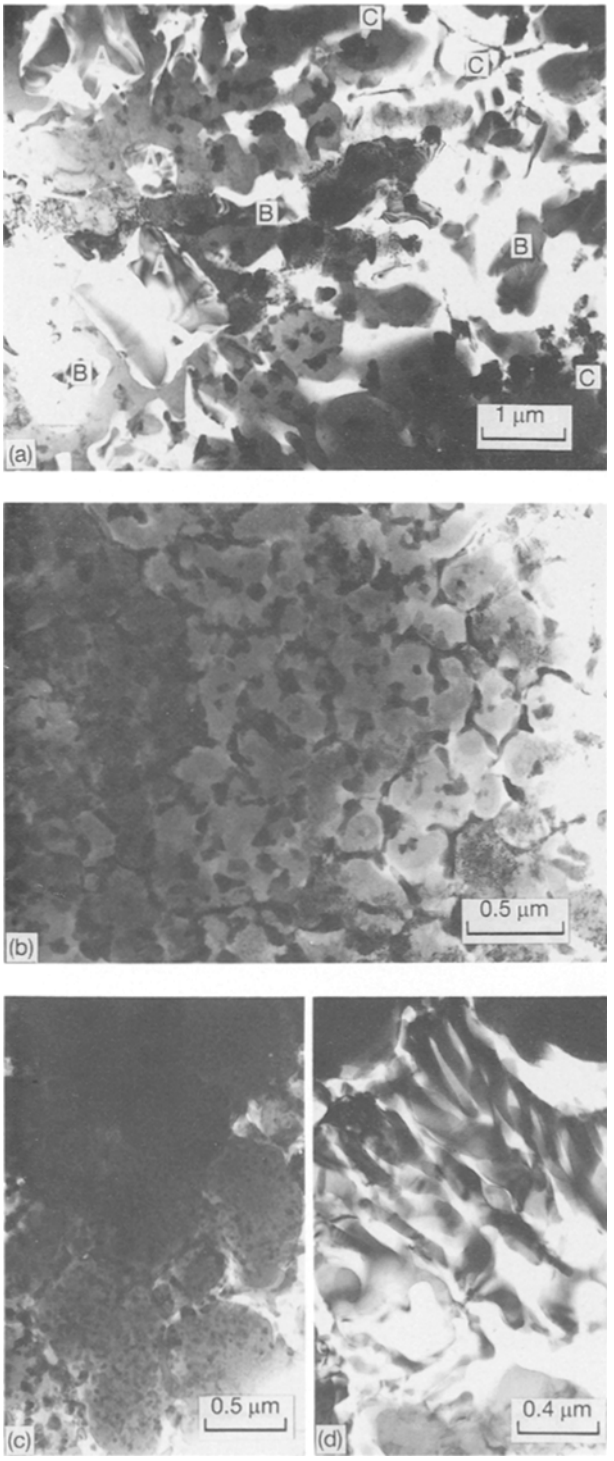


*Figure 4* TEM microstructures of zone B. (a) and (b) an Al–3.5Mn–0.8Co alloy, (c) cells of an Al–3.5Mn–1.3Co alloy, and (d) $Al_6Mn$ dendrites of an Al–3.5Mn–2Co alloy.

A SAD pattern from the TEM image in Fig. 4b revealed the coexistence of the α-Al, icosahedral phase and $Al_9Co_2$. Fig. 4c shows that $Al_9Co_2$ dispersoids were contained in α-Al cells and $Al_6Mn$ particles formed at the cell walls in the Al–3.5Mn–1.3Co alloy. Typical dendrites of $Al_6Mn$ usually show a parallel-like morphology, as seen in Fig. 4d.

Some petal-like branches and α-Al cells are observed in zone B of the Al–5Mn–0.8Co alloy shown in Fig. 5a, and this petal-like branch is the typical morphology of the primary icosahedral phase. Networks along the cell walls are also identified as the icosahedral phase by the SAD pattern showing fivefold symmetry. Moreover, the existence of $Al_6Mn$ particles was also confirmed in this region. In the Al–5Mn–2Co alloy, radially solidified cell grains were observed in a large region, as can be seen in Fig. 5b; this substructure corresponds to the region in the SEM micrograph of Fig. 1e. In Fig. 5b, each grain contained a core, these cores can be identified as particle clusters of the icosahedral phase; and some particles of the $Al_9Co_2$ and $Al_6Mn$ phase which occupy the walls of α-Al cells radiating from the core particles. Moreover, these cells radiate and bifurcate towards the $\langle 0\,1\,1\rangle_{\alpha\text{-Al}}$ directions, and a refined eutectic is found in some intercellular regions.

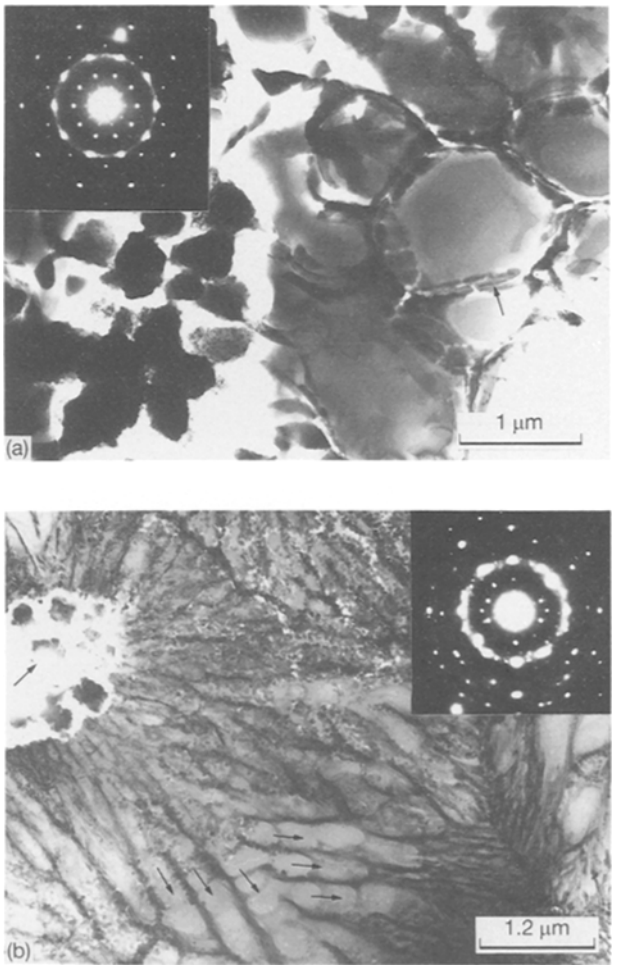


*Figure 5* TEM microstructures of zone B. (a) The Al–5Mn–0.8Co alloy, the fivefold symmetry pattern (indicating the icosahedral phase) is from networks marked by an arrow at the α-Al cell walls. (b) The Al–5Mn–2Co alloy, the SAD pattern is from the core of the icosahedral phase (marked by arrow A).

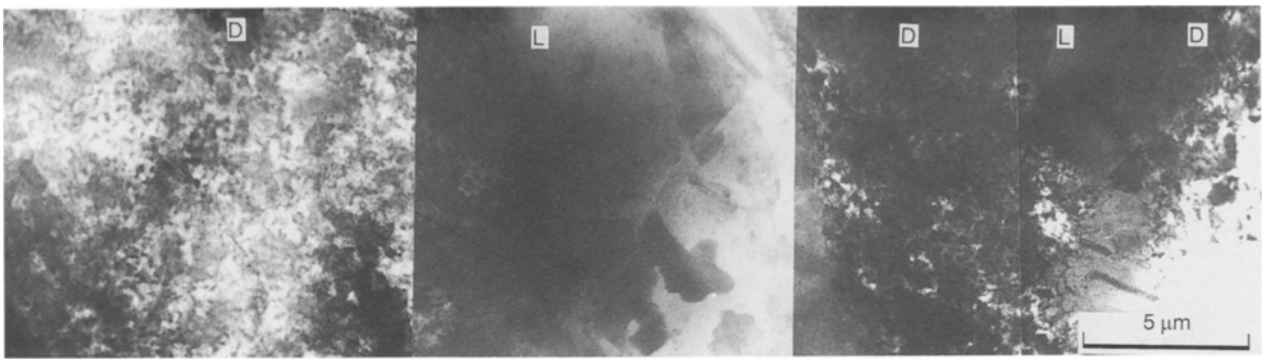


*Figure 6* The TEM microstructure of an alternate arrangement of light and dark bands in the Al–3.5Mn–1.3Co alloy: D denotes the dark band, and L denotes the light band.

### 3.2.3. Banded structure

The alternate appearance of two distinct structural layers was observed in the Al–3.5Mn–1.3Co alloy, as shown in Fig. 6. This structure can be confirmed as a banded structure, and it develops as a transitional structure from zone A to zone B, with reference to the SEM observations in transverse sections of ribbons. The light band consists of columnar grains of α-Al phase with fine $Al_9Co_2$ dispersoids and it has the same structure as zone A, and the dark band is characterized by random α-Al microcells with further large particles of $Al_9Co_2$. This banded structure is different from those in Ag–Cu, Al–Fe and Al–Cu binary alloys [7–12]. In Al–3.5Mn–0.8Co and Al–3.5Mn–2Co alloys, no such alternate arrangement of two layers has been confirmed by TEM observation, despite the SEM structures of the transitional region from zone A to zone B being analogous to those in the Al–3.5Mn–1.3Co alloy.

## 3.3. The $d(\Delta H_0^{ne})/dT$–$T$ curves and values of $\Delta H_0^{ne}$

The $d(\Delta H_0^{ne})/dT$–$T$ curves of the five Al–Mn–Co alloys are illustrated in Fig. 7. The $d(\Delta H_0^{ne})/dT$–$T$ curves of two Al–Mn alloys, quoted from a previous work [16] for comparison, are also shown in Fig. 7. Three obvious peaks, $P_1$, $P_2$ and $P_3$, can be seen on the curves of Al–3.5Mn–2Co, Al–5Mn–0.8Co and Al–5Mn–2Co alloys, however, $P_2$ and $P_3$ are merged into one peak in the Al–3.5Mn–0.8Co and Al–3.5Mn–1.3Co alloys. Peak $P_1$, appeared at temperatures from 540 to 560 K, and it is probably caused by the precipitation and growth of the icosahedral phase. The peaks $P_2$ and $P_3$, in the temperature range 640–800 K, may mainly be induced by the precipitation of an intermetallic compound containing Mn from the supersaturated α-Al solid solution and the transformation from the icosahedral phase to $Al_6Mn$.

The values of $\Delta H_0^{ne}$ and $\Delta H_0^{ne'}$ for the five Al–Mn–Co alloys and the two Al–Mn alloys are summarized in Table II. The values of $\Delta H_0^{ne}$ in the ternary Al–Mn–Co alloys are evidently reduced to a lower level than those in the binary Al–Mn alloys; this can be attributed to the formation of some $Al_9Co_2$ and $Al_6Mn$ particles during rapid solidification. With increasing Co content in Al–Mn alloys, the amount of

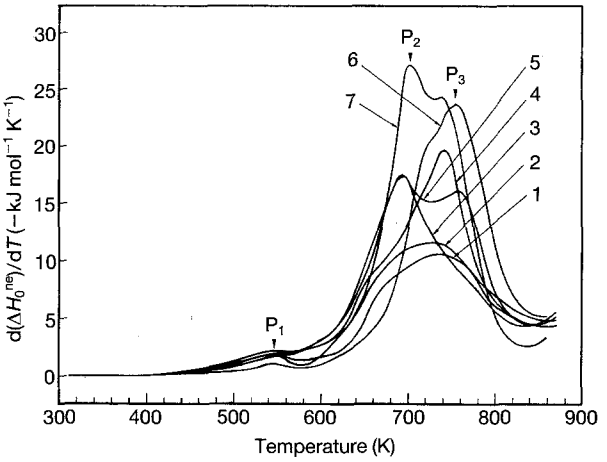


*Figure 7* The $d(\Delta H_0^{ne})/dT$–$T$ curves obtained by DSC measurements during continuous heating at the rate of 0.2 K $s^{-1}$ for: (1) Al–3.5Mn–0.8Co, (2) Al–3.5Mn–1.3Co, (3) Al–3.5Mn–2Co, (4) Al–5Mn–0.8Co, (5) Al–5Mn–2Co, (6) Al–3.95 at % Mn, and (7) Al–5.37 at % Mn.

TABLE II The values of $\Delta H_0^{ne}$ and $\Delta H_0^{ne'}$ (kJ $mol^{-1}$)

| Alloys | $\Delta H_0^{ne}$ | $\Delta H_0^{ne'}$ | $\Delta H_0^{ne} - \Delta H_0^{ne'}$ |
|---|---|---|---|
| Al–3.5Mn–0.8Co | − 2.00 | − 1.08 | − 0.92 |
| Al–3.5Mn–1.3Co | − 2.33 | − 1.23 | − 1.10 |
| Al–3.5Mn–2Co | − 2.55 | − 1.58 | − 0.97 |
| Al–5Mn–0.8Co | − 2.78 | − 1.73 | − 1.05 |
| Al–5Mn–2Co | − 3.08 | − 2.03 | − 1.05 |
| Al–3.95 at % Mn | − 2.82 | − 2.03 | − 0.79 |
| Al–5.37 at % Mn | − 3.28 | − 2.90 | − 0.38 |

$Al_9Co_2$ and $Al_6Mn$ particles increases, and the amount of the icosahedral phase decreases in as-melt spun ribbon. However, the increases in the values of $\Delta H_0^{ne}$ from − 2.00 to − 2.55 kJ $mol^{-1}$ with increases in the Co contents from 0.78 to 2.07 at % is not understood. The values of $\Delta H_0^{ne'}$ are ascribed to the decomposition of the supersaturated α-Al solid solution and the transformation of the icosahedral phase for the Al–3.5Mn–0.8Co and Al–5Mn–0.8Co alloys, and to the decomposition of the supersaturated α-Al phase only for the Al–3.5Mn–1.3Co, Al–3.5Mn–2Co and Al–5Mn–2Co alloys. The values of $\Delta H_0^{ne}$ mainly stem from the values of $\Delta H_0^{ne'}$. The values of $\Delta H_0^{ne} - \Delta H_0^{ne'}$

may be attributed to the formation of a refined microstructure, and for Al–Mn–Co ternary alloys they are larger than those for the Al–Mn binary alloys.

## 4. Discussion

### 4.1. Evolutionary formation of the microstructure

Constrained cooling by the substrate results in the formation of an evolutionary microstructure from the chilled side to the unchilled side in as-melt spun ribbons. The formation mechanism of zone A, a structural region consisting of an α-Al phase with dispersoids of $Al_9Co_2$ and with an icosahedral phase, may be suitable to the model proposed by Cotton and Kaufman [5]. This model presumes that dispersive nuclei of $Al_9Co_2$ and the icosahedral phase initiate in the liquid, and then the α-Al phase nucleates on the substrate surface and rapidly engulfs the dispersoids of $Al_9Co_2$ and the icosahedral phase by plane-front growth. Under such a constrained cooling condition, the nucleation rate of the primary solidified phase becomes very large, thus $Al_9Co_2$ and the icosahedral phase disperse as fine particles and these discrete particles might not cause fluctuations of the plane-front growth of the α-Al phase.

In zone B, the α-Al phase solidifies randomly owing to the reduction of the cooling ability of the substrate; and much $Al_9Co_2$, $Al_6Mn$ and icosahedral phase nucleate at the boundaries of the primary α-Al phase, and some particles may nucleate as primary crystals. These nuclei develop by various morphologies, as can be seen in Figs 4 and 5. In this zone, the cooling rate may be higher than $0.5–2 \times 10^5$ K s$^{-1}$; these values were estimated using the secondary-dendrite-arm spacing in zone B for the Al–Cu-alloy ribbons with thicknesses of 80–120 μm [6].

It is generally considered that the formation of the banded structure is due to an instability in the solidification temperature [7, 8], and Carrard *et al.* [12] recently pointed out that the origin of the banded structure can be understood by considering the undercooling of the solid–liquid interface as a function of the growth rate for dendritic and plane-front growth. The formation of the banded structure will be interpreted in a later section after analysing the thermodynamic aspects of the value of $\Delta H_0^{ne}$, and in this explanation we will take account of the distribution of $\Delta H_0^{ne}$ with the distance from the substrate surface.

### 4.2. Thermodynamic aspects of the value of $\Delta H_0^{ne}$

In a non-equilibrium solidification process, a chemical-potential gradient exists at the solid–liquid interface, and a decrease in the Gibbs free energy, $\Delta G$, must be involved. This Gibbs free energy change, $\Delta G$, is dissipated at the moving interface or it is stored in the solidified solid. This $\Delta G$ can be expressed by Equation 3 for a binary alloy [20, 21]

$$\Delta G = (\mu_A^\alpha - \mu_A^l)(1 - X_B^\alpha) + (\mu_B^\alpha - \mu_B^l)X_B^\alpha \quad (3)$$

where, $\mu_A^\alpha$, $\mu_A^l$, $\mu_B^\alpha$ and $\mu_B^l$ are the chemical potentials of elements A and B in a solidified α-solid and the liquid, and $X_B^\alpha$ is the concentration of element B in the solidified α-solid. This energy should be liberated during heating of the solidified solid and it should induce an exothermic curve in a DSC measurement. Therefore, it can be stated that a predominant part of the value of $\Delta H_0^{ne}$, estimated on the basis of the DSC measurements in the present work, is equal to the decrease in the Gibbs free energy, $\Delta G$, during rapid solidification. This is the thermodynamic aspect of the value of $\Delta H_0^{ne}$. It is very important to note that the moving of the solid–liquid interface at a rapid velocity is accompanied by a large decrease in Gibbs free energy, $\Delta G$, which is ultimately stored in the solidified solid and implies the non-released part of the solidification latent heat.

The values of $\Delta H_0^{ne}$ were already estimated to be $-0.50$, $-1.31$, $-2.82$, $-3.28$ and $-3.49$ kJ mol$^{-1}$ for as-melt spun ribbons of Al–1.66, 2.56, 3.95, 5.45 and 6.98 at% Mn alloys [16], and $-1.90$, $-4.45$ and $-4.59$ kJ mol$^{-1}$ for as-melt spun ribbons of Al–6.74, 8.48 and 11.97 at% Si alloys [22], respectively. These values of $\Delta H_0^{ne}$, so large amount of non-released latent heat, cannot be neglected on discussion of the rapid-solidification process, because the latent heat of the pure Al is only 10.47 kJ mol$^{-1}$.

The value of $\Delta H_0^{ne}$ can be attributed to the formation of a non-equilibrium phase and a fine structure during rapid solidification. The value of $\Delta H_0^{ne'}$, the major part of $\Delta H_0^{ne}$, is ascribed to the formation of metastable phases, and the value of $\Delta H_0^{ne} - \Delta H_0^{ne'}$ is attributed to an extremely refined microstructure. In as-melt spun ribbons of the above mentioned Al–Si alloys, only a supersaturated α-Al phase was detected by X-ray diffraction (XRD), and the value of $\Delta H_0^{ne'}$, estimated from the area integration of an exothermic peak of a Si-phase precipitation, is in good agreement with the heat of solution, which was calculated by Soma *et al.* [23] using a microscopic electronic theory based on pseudopotentials and the virtual crystal approximation. The values of $\Delta H_0^{ne'}$, ($-0.35$, $-0.43$ and $-0.57$ kJ mol$^{-1}$ for as-melt spun ribbons of Al–28.1, 28.8 and 30.4 at% Cu alloys, respectively [24]) can be ascribed to the formation of a non-equilibrium intermetallic compound $Al_2Cu$ phase, because the exothermic peak on the $d(\Delta H_0^{ne})/dT$–$T$ curve implies the enthalpy change for the transformation from a non-equilibrium $Al_2Cu$ to the equilibrium $Al_2Cu$ plus α-Al phases. Thus, $\Delta H_0^{ne}$ is also a driving force for the transformation from the non-equilibrium state of the as-rapidly-solidified alloy to the equilibrium state of the fully annealed alloy.

Equation 3 can also be written as [20]

$$\frac{\Delta G}{RT} = \frac{(1 - k_v X_1) X_1 (k - k_v)}{1 - k X_1} + k_v X_1 \ln\left(\frac{k_v}{k}\right) \quad (4)$$

where, $X_1$ is the alloy composition, $k$ is the equilibrium distribution coefficient and $k_v$ is the non-equilibrium distribution coefficient. When the temperature of the interface is below $T_0$, a critical temperature below which the interface proceeds with no solute partitioning, *partitionless solidification* occurs with $k_v = 1$ and this results in the formation of a supersaturated solid

solution. When a second phase forms with $k_v < 1$ at a temperature $T$ which is higher than $T_0$, $\Delta G$ differs from the value for the case of partitionless solidification. The relationship between $\Delta G$ and the moving velocity of the interface, $V$ can be expressed by [20, 25]

$$V = V_c\left[1 - \exp\left(\frac{\Delta G}{RT}\right)\right] \quad (5)$$

where, $V_c$ is a kinetic rate parameter for crystallization. It can be considered that the value of $\Delta G$ at the interface varies with the distance from the chilled surface for the ribbons of two-zone structure in binary Al alloys, and that the distribution of $\Delta H_0^{ne}$ and the change in the moving velocity of the interface is dependent on the cooling ability of the substrate. Thus, a larger value of $\Delta G$ (negative) should be stored, and a larger moving velocity of the interface should be taken at the chilled side than at the unchilled side during rapid solidification. These considerations should also be valid in as-melt spun ribbons of ternary Al–Mn–Co alloys.

## 4.3. Formation of the banded structure

The formation of the banded structure can be connected with the decrease in Gibbs free energy, $\Delta G$, at the moving solid–liquid interface, as well as with the value of $\Delta H_0^{ne}$. We will consider the formation of the banded structure in a binary Al alloy ribbon on this basis. Fig. 8a schematically shows a regular banded structure in a transverse section of the ribbon of a binary Al alloy; this banded region is sandwiched between a supersaturated α-Al phase at the chilled side and a two-phase region at the unchilled side. The banded structure consists of a periodical arrangement of α-Al light bands and two-phase dark bands, the first thin band to appear is dark, and the following light band is the thickest. According to Zimmermann *et al.* [10], the relative volume fraction of the light bands should decrease slightly and that of the dark bands should increase slightly; however, the width of each pair of the dark and light bands should be constant.

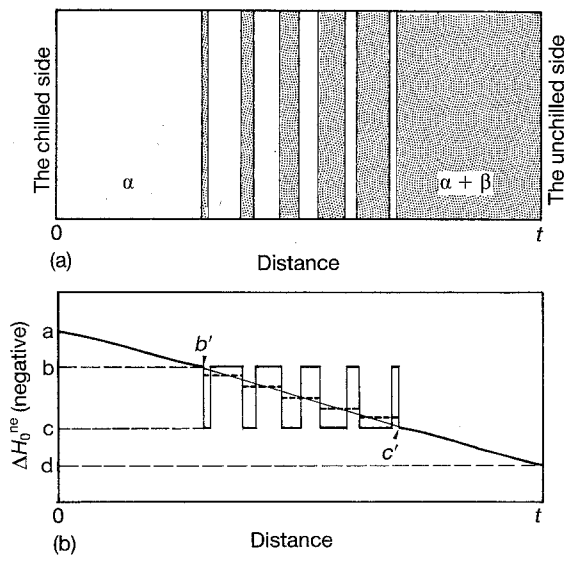


*Figure 8* (a) A schematic diagram of the banded structure, (b) the oscillatory curve of the distribution of $\Delta H_0^{ne}$.

This evolutionary structure suggests that the decrease in Gibbs free energy, $\Delta G$, at the solid–liquid interface fluctuates from the chilled to unchilled surface during rapid solidification, and the distribution of $\Delta H_0^{ne}$ in the solidified solid must correspond to the fluctuation of $\Delta G$. Fig. 8b illustrates the distribution of $\Delta H_0^{ne}$ by the solid line, which corresponds to the fluctuation of $\Delta G$ at the interface and is dependent on the distance from the substrate during rapid solidification. The maximum value of $\Delta H_0^{ne}$ (negative) is $\Delta H_0^{ne}$ ($a$) at the chilled surface and the minimum value (negative) is $\Delta H_0^{ne}$ ($d$) at the unchilled surface. Because a supersaturated α-Al phase constituting the light bands is formed by partitionless solidification with $k_v = 1$ and at $T < T_0$, $\Delta G$ at the interface should be $|\Delta G| > |\Delta G(b)|$, and $\Delta G(b)$ can be expressed as

$$\Delta G(b) = RT_0\left[\frac{(1 - X_1)X_1(k - 1)}{1 - kX_1} + X_1 \ln\left(\frac{1}{k}\right)\right] \quad (6)$$

Two phases were formed in dark bands with $k_v = k'_v < 1$ and $T = T' \geqslant T_0$, and then the decrease in Gibbs free energy, $\Delta G$ at the interface should be $|\Delta G| \leqslant |\Delta G(c)|$, and $\Delta G(c)$ can be written as

$$\Delta G(c) = RT'\left[\frac{(1 - k'_vX_1)X_1(k - k'_v)}{1 - kX_1} + k'_vX_1 \ln\left(\frac{k'_v}{k}\right)\right] \quad (7)$$

A critical energy is necessary for existence of the particles of the second phase in the α-Al phase, this energy indicates an energy difference between both light and dark bands, satisfying

$$|\Delta G(b)| - |\Delta G(c)| \geqslant |\Delta G_n| \quad (8)$$

where $\Delta G_n$ is the critical activation energy for the nucleation of the second phase. As a result, an oscillatory curve of the distribution of $\Delta H_0^{ne}$ can be drawn for the banded region. Two threshold values, $\Delta H_0^{ne}(b)$ and $\Delta H_0^{ne}(c)$, relate to the values of $\Delta G(b)$ and $\Delta G(c)$, respectively. According to Equation 5, the growth velocity of the light bands should be larger than that of the dark bands.

Despite the oscillation in the distribution of $\Delta H_0^{ne}$, the total value of $\Delta H_0^{ne}$ (negative) in the coupled light and dark bands should gradually reduce from the threshold value $\Delta H_0^{ne}(b)$ to the threshold value $\Delta H_0^{ne}(c)$ with increasing distance from the chilled surface, as is shown by the dashed line in Fig. 8b. If the total width of two coupled light and dark bands decreases infinitely, the total value of $\Delta H_0^{ne}$ in the coupled bands could change along the straight line $b'$–$c'$, as shown in Fig. 8b; this line undoubtedly indicates a gradual reduction of the cooling ability of the substrate with distance from the cooling substrate.

Therefore, the formation of the banded structure in binary Al alloys can be understood on the following basis. Because of the existence of a critical activation energy for the nucleation of the second phase, the

decrease in Gibbs free energy, $\Delta G$, at the interface oscillates in order to correspond with the gradual reduction of the cooling ability of the substrate from the chilled side to the unchilled side, and this results in a relevant oscillation of the solidification temperature and in the moving velocity of the interface. If the heat capacity of the Al alloy is taken to be equal to $31.748\ J\ K^{-1}\ mol^{-1}$, which is the heat capacity of pure Al liquid [26], the oscillation of $\Delta G$ of $0.31748\ kJ\ mol^{-1}$ should cause a temperature oscillation of about 10 K for the molten alloy. In fact, for an Al–2 wt% Fe alloy, the temperature oscillation of the solid–liquid interface necessary to form the banded structure has been calculated by Gremaud *et al.* [11] to be only about 5 K.

The formation sequence of the banded structure by the alternate recalescence can be described as follows. (i) The supersaturated α-Al phase forms by plane-front growth near the chilled surface at a large growth velocity and at a temperature lower than $T_0$. In this case, the decrease in Gibbs free energy, $\Delta G$ (negative), is larger than $\Delta G(b)$, and almost all of the released heat is extracted by a cooling substrate; a small amount of the released heat, termed the *back flux of released heat*, flows into the liquid. (ii) The first dark band is formed upon the collapse of the plane-front growth at an interface temperature higher than $T_0$, and at a small growth velocity. The interface temperature is elevated by the back flux of released heat, and the small growth velocity provides sufficient time for the substrate to extract all the released heat. Thus, $\Delta G$ deviates from the $b'-c'$ line and coincides with $\Delta G(c)$. (iii) The formation of the first light band cooperates with the first dark band as a pair, so that the change of the total $\Delta G$ of a pair of dark and light bands approaches the $b'-c'$ line. Thus, the first light band is formed with a rapid growth at a lower temperature than $T_0$, meanwhile, the back flux of released heat flows into the liquid. (iv) Owing to the back flux of released heat and a gradual reduction in the cooling ability of the substrate, the second dark band, which is the thicker band, forms by the recalescence of liquid at the front of the first light band. Such an alternative formation sequence should proceed until the total $\Delta G$ of a pair of bands coincides with another threshold value, $\Delta G(c)$.

Although the banded structure in the Al–Mn–Co alloys is different from that in a binary Al alloy, the formation mechanism may be the same as that in binary Al alloys; that is, the dark bands were formed at a high temperature and with a low moving velocity of the interface, and the light bands were formed by plane-front growth at the low temperature and a high growth rate of the interface. The formation of both the bands would involve different decreases in Gibbs free energy, $\Delta G$. However, the two threshold values, $\Delta G(b)$ and $\Delta G(c)$, have a different significance from the case of binary Al alloys: $\Delta G(b)$ is the minimum $\Delta G$-value for producing columnar α-Al grains containing $Al_9Co_2$ dispersoids, and $\Delta G(c)$ is the maximum $\Delta G$-value for producing microcells of the α-Al phase containing large $Al_9Co_2$ particles. Between these two threshold values, the fluctuation of $\Delta G$ or the distribution of $\Delta H_0^{ne}$ will oscillate in order to correspond with the gradual reduction in the cooling ability of the substrate.

## 5. Conclusions

1. As-melt spun ribbons of Al–3.5Mn–0.8Co, Al–3.5Mn–1.3Co, Al–3.5Mn–2Co, Al–5Mn–0.8Co and Al–5Mn–2Co alloys exhibit an evolutionary microstructure consisting of two zones, zone A and zone B, and the banded structure is observed as a transitional region between zone A and zone B in the Al–3.5Mn–1.3Co alloy. Zone A contains directionally solidified α-Al grains with dispersoids of $Al_9Co_2$ and icosahedral phases formed at the chilled side, and zone B consists of randomly-solidified α-Al cells with dendrites of the intermetallic compounds formed at the unchilled side.

2. Because of the formation of $Al_9Co_2$ dispersoids, the rapidly solidified Al–Mn–Co alloys reveal lower values in the enthalpy difference, $\Delta H_0^{ne}$, than those in the rapidly solidified Al–Mn binary alloys. The value of $\Delta H_0^{ne}$ should correspond to a decrease in Gibbs free energy, $\Delta G$, which is dissipated at the moving interface or is stored in the solidified solid during rapid solidification.

3. A decrease in Gibbs free energy, $\Delta G$, at the moving solid–liquid interface oscillates between two threshold values, $\Delta G(b)$ and $\Delta G(c)$ corresponding to the initiation and termination of the bands, in order to correspond with a gradual reduction in the cooling ability of the substrate. Such an oscillatory variation of $\Delta G$ provides relevant oscillation of the temperature and moving velocity of the interface for rapid solidification and results in the formation of the banded structure.

## Acknowledgements

Yibin Zhang acknowledges the Japanese government (the Ministry of Education, Science and Culture) for a scholarship and is grateful to Mr Y. Sato for supporting the operation of the transmission electron microscope.

## References

1. H. JONES, *Mater. Sci. Engng.* **5** (1969/70) 1.
2. W. J. BOETTINGER, L. BENDERSKY and J. G. EARLY, *Metall. Trans. A* **17** (1986) 781.
3. W. J. BOETTINGER, L. BENDERSKY, R. J. SCHAEFER and F. S. BIANCANIELLO, *ibid. A* **19** (1988) 1101.
4. L. A. BENDERSKY, A. J. McALISTER and F. S. BIANCANIELLO, *ibid. A* **19** (1988) 2893.
5. J. D. COTTON and M. J. KAUFMAN, *ibid. A* **22** (1991) 927.
6. Y. ZHANG, T. YAMANE, K. HIRAO and Y. MINAMINO, *J. Mater. Sci.* **26** (1991) 5799.
7. D. G. BECK, S. M. COPLEY and M. BASS, *Metall. Trans. A* **12** (1981) 1687, and *A* **13** (1982) 1879.
8. W. J. BOETTINGER, D. SHECHTMAN, R. J. SCHAEFER and F. S. BIANCANIELLO, *ibid. A* **15** (1984) 55.
9. A. KAMIO, H. TEZUKA, T. SATO, THAN TRONG LONG and T. TAKAHASHI, *J. Jpn. Inst. Light Metals* (in Japanese) **35** (1985) 275.
10. M. ZIMMERMANN, M. CARRARD, M. GREMAUD and W. KURZ, *Mater. Sci. Engng. A***134** (1991) 1278.

11. M. GREMAUD, M. CARRARD and W. KURZ, *Acta Metall.* **38** (1990) 2587, **39** (1991) 1431.
12. M. CARRARD, M. GREMAUD, M. ZIMMERMANN and W. KURZ, *ibid.* **40** (1992) 983.
13. D. SHECHTMAN, R. J. SCHAEFER and F. S. BIANCANIELLO, *Metall. Trans. A* **15** (1984) 1987.
14. K. YU-ZHANG, M. HARMELIN, A. QUIVY, Y. CALVAYRAC, J. BIGOT and R. PORTIER, *Mater. Sci. Engng.* **99** (1988) 385.
15. J. A. JUAREZ-ISLAR, D. H. WARRINGTON and H. JONES, *J. Mater. Sci.* **24** (1989) 2076.
16. Y. ZHANG, T. YAMANE, S. SAJI and J. TAKAHASHI, *J. Mater. Sci.* **28** (1993) 3235.
17. T. OHASHI, L. DAI and N. FUKATSU, *Metall. Trans. A* **17** (1986) 799.
18. L. A. BENDERSKY, F. S. BIANCANIELLO, S. D. RIDDER and A. J. SHAPIRO, *Mater. Sci. Engng. A***134** (1991) 1098.
19. K. F. KOBAYASHI, H. KAWAURA and P. H. SHINGU, in "Aluminum alloys – their physical and mechanical properties", Vol. 1, edited by E. A. Starke and T. H. Sanders (EMAS, Warley, 1986) p. 247.
20. W. KURZ and D. J. FISHER, in "Fundamentals of solidification" (Trans Tech Publications, Aedermannsdorf, Switzerland, 1986) p. 220.
21. J. C. BAKER and J. W. CAHN, in "Solidification" (American Society for Metals, Metals Park, OH, 1971) p. 23.
22. Y. ZHANG, T. YAMANE, S. SAJI and J. TAKAHASHI, *Met. Trans.* in press.
23. T. SOMA, Y. FUNAYAMA and H. KAGAYA, *J. Mater. Sci.* **25** (1990) 3917.
24. Y. ZHANG, Y. YAMANE and J. TAKAHASHI, *J. Mater. Sci. Lett.* **11** (1992) 155.
25. W. J. BOETTINGER and M. J. AZIZ, *Acta Metall.* **37** (1989) 3379.
26. I. BARIN, "Thermochemical data of pure substances" (VCH, Weinhein, 1989) p. 17.

*Received 30 October 1992*
*and accepted 8 October 1993*